Dyes and Pigments 141 (2017) 53–65

Contents lists available at ScienceDirect

Dyes and Pigments

journal homepage: www.elsevier.com/locate/dyepig

Pigment-size effect on the physico-chemical behavior of azurite-tempera dosimeters upon natural and accelerated photo aging

Carolina Cardell [a, *], Agustín Herrera [a], Isabel Guerra [b], Natalia Navas [c], Luis Rodríguez Simón [d], Kerstin Elert [a]

[a] Dept. of Mineralogy and Petrology, Faculty of Science, University of Granada, Campus Fuentenueva s/n, E 18071 Granada, Spain
[b] Scientific Instrumentation Centre, University of Granada, Campus Fuentenueva s/n, E 18071 Granada, Spain
[c] Dept. of Analytical Chemistry, And Biomedical Research Institute of Granada (IBIG), Faculty of Science, University of Granada, Campus Fuentenueva s/n, E 18071 Granada, Spain
[d] Dept. of Paint and Restoration, Faculty of Fine Arts, University of Granada, Av. Andalucía s/n, 18071 Granada, Spain

ARTICLE INFO

Article history:
Received 17 October 2016
Received in revised form
21 December 2016
Accepted 2 February 2017
Available online 4 February 2017

Keywords:
Azurite pigments
Glue binder
Paint dosimeters
Particle size
Photo-aging tests

ABSTRACT

This paper presents the first comprehensive study on the role played by pigment particle size in pigment-binder interactions, and thus susceptibility to aging of azurite-rabbit glue paint dosimeters upon accelerated UV-aging *versus* outdoor sunlight exposure. A complementary multi-analytical approach, including spectroscopic and surface analytical techniques, was applied to characterize commercial azurite pigments, as well as blank and aged dosimeters. Results show the crucial role played by azurite particle size on protein-copper complex formation, which governed physico-chemical properties of paints and their aging behavior under different light-aging conditions. On UV-aged dosimeters, finer particles promoted stronger binder structural changes, inducing more severe color changes ($\Delta E = 6–17$). Azurite size also controlled crack formation which was more severe as pigment grain increased due to greater accumulation of binder in inter-pore spaces. Outdoor exposure caused important binder loss (50–60%) and initial transformation of azurite into malachite. Since analyzed pigment composition and particle size differed from manufacturer data, we recommend their characterization prior to use in conservation works and scientific studies. Based on these results, paints made of coarse azurite particles are preferable since they are less prone to color change. Moreover, a small addition of fine-grained pigments might reduce crack development upon aging.

1. Introduction

The increasing interest in historical painting techniques and artist materials over recent decades has led to numerous publications dealing with the use and characterization of traditional painting materials, i.e., in-/organic pigments and organic binders, utilized prior to the 18th century. Research on these materials is key to: i) unravel artistic and technical issues of historic paintings [1–4], ii) establish dating, authorship or forgery of artworks [5–8], iii) understand aging mechanisms [9–13], and thus, iv) promote preventive conservation strategies and suitable conservation/restoration treatments [14–16].

To investigate damage processes, model paint samples (dosimeters or mock-ups), that mimic the composition and structure of real paintings, are often used to evaluate the effects of temperature (T), relative humidity (RH), ultraviolet/visible (UV/Vis) irradiation, and pollutant gases and particles, through in situ and/or accelerated aging tests [10,17–20]. Sunlight is particularly important in promoting physico-chemical reactions on paintings causing fading or darkening [21–23]. Thus, in countries where the incidence of solar light is significant, such as those of the Mediterranean Basin, light-induced decay on paint artworks is an important issue to take into account.

Light-induced damage to a great variety of dyes, pigments and organic binders has been the topic of many investigations over the last decades [23–25]. Only more recently studies have tackled the paintings aging considering the interaction between pigments and binders [10,13,18,19]. For instance, Odlyha et al. [18] examined the effect of accelerated and natural indoor light aging on azurite-egg-yolk tempera dosimeters. They found that azurite induced binder

* Corresponding author.
E-mail address: cardell@ugr.es (C. Cardell).

http://dx.doi.org/10.1016/j.dyepig.2017.02.001
0143-7208/

oxidation although dosimeters suffered only minor changes in their thermal stability upon light aging. Manzano et al. [10] also detected slight changes in reflectance values of azurite-rabbit glue tempera dosimeters exposed to accelerated UV-aging. These changes were not influenced by the different binder amount present in the tempera paints.

To further elucidate the pigment-binder interaction on the weathering behavior of azurite tempera (i.e., color changes, pigment and binder composition, and texture of paint dosimeters), we have included azurite pigments of various particle sizes in this study. The effect of particle size on pigment features (e.g. color, hiding power, appearance and optimum surface finish) is widely recognized [26–29]. However, the contribution of pigment size on paint alteration has seldom been addressed [27]. Hence, in this work azurite-rabbit glue tempera dosimeters were exposed to artificial UV light (laboratory aging test) and outdoor sunlight radiation (two-year outdoor test in Granada, South Spain) in order to gain knowledge about similarities and discrepancies in their photophysicochemical decay.

Long-term outdoor exposure was performed since previous studies mainly focused on photodegradation of pigments and paints under controlled indoor/museum conditions [17,18] and results are not easily applicable to wall paintings and polychrome artworks located in (semi)-open monuments/buildings exposed to the Mediterranean climate. These are part of many important monuments of Granada, including the known worldwide Alhambra and Generalife [1,4,7,14] and the wall paintings in the *Carrera del Darro* [30]. Their state of conservation varies greatly and the here obtained results will serve as the basis for the determination of prevailing degradation mechanisms and the selection of suitable materials for their restoration. Prior to aging tests, the selected commercial azurite pigments were fully characterized. On all samples an array of complementary spectroscopic and surface analytical techniques were applied.

2. Materials and methods

2.1. Materials

Azurite ($Cu_3(CO_3)_2(OH)_2$) was the most widely used blue pigment in European paintings from the 15th to the middle of the 17th century [31]. Traditionally, azurite has been used coarsely ground since it becomes pale and unsuitable as a coloring material when very finely ground [32]. In 1997 Michel Price (MP) developed a method for the separation of ground azurite into different pigment sizes corresponding to diverse hues of blue, from a deep rich blue to a pale sky blue [28]. This method consists of consecutive washings in an egg yolk medium, separating different particle sizes based on Stokes' law. This treatment also confers to azurite protection against acid reactions in oil media by surrounding pigment particles with a protein coating. In 1998 Kremer Pigments GmbH & Co. KG adopted this method to prepare a new range of azurite pigments, called “azurite MP.” These pigments are available in seven grades (according to their average particle size) from a deep royal blue to a pale sky blue.

In this study we analyzed Kremer azurite pigments with different particle sizes which include various “azurite MP” and the “azurite natural standard” (color index PB3077420) (Table 1). Pearls of rabbit glue (Kremer Pigments GmbH & Co. KG, ref. 63028) were used to prepare proteinaceous-based paint dosimeters. The binder was prepared according to traditional recipes. Eight grams of rabbit glue were soaked in 100 ml of deionized water for 24 h, under periodic stirring. Afterward the mixture was heated below 50 °C in a water bath and stirred to obtain a homogeneous mixture. The rabbit glue was cooled to room T (22 °C) until a gel-like consistency was obtained.

2.2. Paint dosimeters preparation

During the Middle Ages and the Renaissance, pigments were ground into particles of properly uniform size to obtain a smooth spreading paint. Afterward the pigments were mixed with the correct amount of binder to make an easily workable paint. Though there are manuscripts, treatises and books with painting recipes [33–35], in practice the precise amount of binder to be mixed with a pigment varied since it depends on the crystal size attained during the pigment grinding.

Hence, in this work the paint dosimeters were prepared according to traditional procedures, used by medieval painters, considering organoleptic parameters. Each pigment was first mixed with deionized water. Then, droplets of prepared rabbit glue were added until an adequate consistency was reached. It was found adequate when droplets formed at the tip of the brush would not fall off easily. Subsequently, several layers of paint mixture were applied by brush to glass slides (76 × 26 × 1mm). Care was taken that each layer be completely dry before the next was applied. Then, glass slides were cut with a diamond knife into 15 × 15 × 1 mm pieces to conduct the aging tests. To obtain the pure rabbit glue binder dosimeter, the glue paste was directly applied onto the glass slide.

Paint dosimeters are named adding the letter C (which refers to rabbit glue, *cola* in Spanish) to the pigments label (see Table 1), to clearly differentiate powder pigments from binary (pigment/binder) paint mixtures.

2.3. UV-accelerated aging test

The artificial aging test was performed during 1000 h in a ventilated chamber at 24 ± 3 °C and 25 ± 10% RH. A tubular UV lamp (TL 40W/12 RS SLV/25, Philips Lighting Holding B.V.) was operated continuously during the test. The lamp emits more than 85% of its energy in the UV-B wavelength range with a peak at ~320 nm. Irradiance level was fixed at 765 W/m^2. Day light was blocked using aluminum foil.

2.4. Outdoor sunlight exposure test

The paint dosimeters were placed vertically in an exterior eave (protected from direct rainfall) of the Granada Cathedral (South Spain), in the historic center of the city where traffic is restricted. Samples faced SW and were exposed for two years to direct sunlight ~5 h in winter and ~10 h in summer, under urban air conditions. It was estimated that the overall sunlight exposure duration was ~5500 h at an irradiance level of ~1090 W·m^{-2} [36]. During the exposure, T reached 40 °C in summer and −3 °C in winter (www.ugr.es/~velilla/meteo-albayzin/resumen.htm, accessed 7.7.16). The average maximum T in Granada being ~30–35 °C in summer and ~10–15 °C in winter, with diurnal variations up to 20 °C. The average RH was ~40% in summer and ~75% in winter, with average monthly precipitation ranging from ~5 mm in summer to ~40 mm in winter (www.granada.climatemps.com, accessed 5.7.16). Data on average concentrations of atmospheric aerosols during winter and summer 2015 are reported in Table 2. Although Granada is a non-industrialized city, concentrations of NO_2, O_3 and particulate matter with 10 μm average size (PM_{10}) in 2015 frequently exceeded the threshold values set by the EU directive 2008/50EC. The SO_2 concentration was generally below the established limit. Particle matter is primarily constituted by soil dust (quartz, calcite, dolomite, phyllosilicates, iron oxides/hydroxide), black carbon, secondary inorganic aerosols, and sea salt [14,37].

Table 1
Characteristics of commercial azurite pigments.

Kremer pigment reference	Stereomicroscope image of pigments scale: 0.6 mm	Kremer pigment size	Authors azurite reference
Azurite MP extra deep. No. 10203 (intense dark blue)	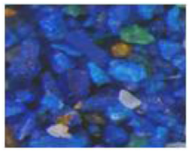	80-100 μm	AZ-EC: azurite extra coarse
Azurite MP, deep. No 10204 (dark blue)	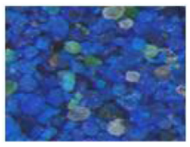	63-80 μm	AZ-C: azurite coarse
Azurite MP, pale, No 10206 (light blue)	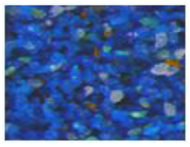	38-63 μm	AZ-M: azurite medium
Azurite MP, sky-blue. No K10207 (light greenish blue)	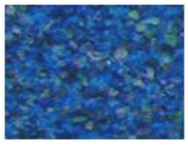	<38 μm	AZ-EF: azurite extra fine
Azurite standard. No 10200 (deep greenish blue)	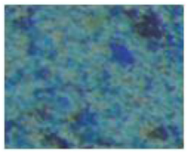	<120 μm	AZ-ST: azurite standard

Table 2
Average air contamination and particulate matter (PM_{10}) concentration ($\mu g \cdot m^{-3}$) during winter and summer 2015 in the city center of Granada.

Dates	SO_2	NO_2	O_3	PM_{10}
15/1/2015-29/1/2015	15.8 ± 6.1	40.2 ± 21.0	31.6 ± 22.7	22.2 ± 14.3
22/6/2015-8/7/2015	6.9 ± 7.0	29.9 ± 21.7	82.5 ± 31.1	40.6 ± 20.1

Data from www.juntadeandalucia.es/medioambiente/site/rediam/menuitem, 1.12.16.

2.5. Analytical techniques

The azurite pigments, organic binder, and all paint dosimeters (i.e. blank and aged) were analyzed with the following analytical techniques:

A stereomicroscope (SMZ 1000, Nikon) was used to examine the textural, structural and chromatic features of blank and aged paint dosimeters. Granulometry (Mastersizer 2000LF, Malvern Instruments) was performed to verify the particle size of the azurite pigments in the range 0.02–1500 μm using laser diffraction. Samples were dispersed in ethanol. Thermogravimetric analysis (TG) was used to quantify both the egg yolk present in the commercial azurite pigments and the rabbit glue binder added to each azurite to prepare the corresponding paint dosimeter. Analyses were performed on a Shimadzu TGA-50H (Shimadzu Corporation) in flowing air (100 ml/min) at a constant heating rate of 10 °C min^{-1} (25–950 °C). One analysis per sample was performed. The binder content of paint dosimeters was calculated considering the weight loss of the corresponding azurite pigment and the pure binder in the same temperature range. Using X-ray diffraction (X'Pert PRO PANalytical B.V.), the mineralogical composition of azurite pigments and all paint dosimeters was identified. Analyses were performed using Cu-Kα radiation, Ni filter, 45 kV voltage, 40 mA intensity and spinner. The exploration range was 3° to 60° 2θ and goniometer speed 0.05° 2θ s^{1}. Identification and semi-quantification (~5%) of minerals were carried out using Xpowder [38].

To analyze the micro-texture and chemical composition of pigments and all paint dosimeters, two high-resolution (Schottky-type field emission) scanning electron microscopes (FESEM) coupled to an energy dispersive X-ray spectrometer (EDX) were used. Samples were mounted on Al stubs with double-sided adhesive C tape. The instruments were: i) an Auriga (Carl Zeiss, Germany) joined to an INCA-200 EDX working at 10^{-4} Pa vacuum and 2 kV beam accelerating voltage (secondary electron imaging mode; carbon-coated samples); and ii) a variable pressure FESEM (VP-FESEM, Supra 40Vp Carl Zeiss, Germany) equipped with an Aztec 3 EDX and X-Max 50 mm detector. Working conditions were 40–66 Pa vacuum, 15–20 kV (imaging mode) and 20 kV beam accelerating voltage (samples not carbon coated). High-resolution X-ray maps (1024 × 768 pixels) were obtained from selected areas with 100 frames and a dwell time of 10 ms (2.5 h acquisition) using 3 nA filament current and 20 eV/ch resolution. To determine the nature of the crystalline/amorphous phases present in the dosimeters, phase maps were compiled from elemental distribution maps by applying the *Find Phases* tool implemented in the Aztec 3 version used in this work. This procedure allowed us to highlight the location, morphology and amount of phases present in the

paint dosimeters. Linear crack density (mm^{-1}) was calculated using 0.1 × 0.095 mm^2 SEM images according to the following equation: crack length (mm)/image size (mm^2) = linear crack density (mm^{-1}).

A portable reflectance spectrophotometer (Minolta CM-700D) was used to measure the chromatic features of the paint dosimeters. Color data were collected in SCI (specular component included) and SCE (specular component excluded) modes from 400 to 700 nm at 10 nm intervals for the standard D65 daylight illuminant (color temperature 6504 K) using 10° observer and an 8 mm measuring aperture. Note that the difference between SCI and SCE measurements was ≤0.2 units for all color parameters, and only the former are reported in this study. Data were expressed in the CIE L*a*b* and CIE h*C*L* color spaces. In the CIE L*a*b* system, L* is luminosity which varies from black with a value of 0 to white with a value of 100; a* varies from +a* (red) to −a* (green) and b* ranges from +b* (yellow) to −b* (blue). In the CIE h*C*L* color system each color is represented by three cylindrical coordinates: hue or tone (h*) which refers to the dominant wavelength, chroma or saturation (C*) related to the intensity of color, and L* which is lightness or luminosity of color. The CMC (2:1) version of the color difference formula (i.e., $\Delta E = \sqrt{(\Delta L^*)^2+(\Delta a^*)^2+(\Delta b^*)^2}$) was used to colorimetrically compare dosimeters [39]. In general terms, these differences will be visually perceptible when the values change by more than three units [40]. Average values are based on a minimum of 5 measurements per samples.

A confocal Raman spectrometer (Jasco NRS-5100) fitted with an Olympus microscope and a Peltier-cooled CCD detector (Andor DU 420 OE) was used to recognize the molecular composition of powder pigments, rabbit glue binder and all the paint dosimeters. Samples were observed using the 5X, 20X and 100X objectives. The video camera was used to identify particular locations in the samples, which were excited with lasers at 532 nm (green, Elforlight G4-30; Nd:YAG) and 785 nm (red, Torsana Starbright). The scattered Raman light was collected in a 180° backscattering geometry by a Charge Coupled Device (CCD) after having passed through a 50 μm entrance slit. Spectra were collected with an average resolution of 2 cm^{-1} within the wavenumber range of 100–3000 cm^{-1}. To improve the signal/noise ratio and avoid laser-induced degradation of samples, a series of recorded spectra (n = 6–10) were collected from each sample spot and averaged, with exposure times from 20 to 30s for green (100% power, Max Power Density $W{\cdot}cm^{-2} = 6.37e^{-7}$), and from 30 to 40s for red laser (10% power, Max Power Density $W{\cdot}cm^{-2} = 8.40e^{-8}$). To ensure statistical representativity, a minimum of 5 spots were analyzed in each sample.

Attenuated Total Reflection − Fourier transform infrared spectroscopy (ATR-FTIR) was performed on powder samples of pigments and binder, as well as on blank and aged dosimeters using a Jasco 6200 (JASCO Analytical Instruments, Japan). The dosimeters were pressed against the ATR diamond crystal window and the infrared (IR) spectra were recorded at a 2 cm^{-1} resolution over 100 scans from 400 to 4000 cm^{-1}. The ATR correction was applied on selected FTIR spectra using Spectra Manager II software. Results showed no peak shifts as compared to uncorrected FTIR spectra. The results reported here are based on uncorrected ATR-FTIR data.

3. Results and discussion

3.1. Stereomicroscope study of paint dosimeters

The stereomicroscope images revealed that all azurite pigments contained impurities, showing colorless and green colored crystals (Fig. 1), identified as quartz (SiO_2) and malachite ($Cu_2(CO_3)(OH)_2$ using XRD (see section 3.4). Additionally, a few orange-brown/black crystals were observed and recognized as iron oxides/hydroxides (Fig. 1h) with VP-FEMEM-EDX (see section 3.5). In AZ-ST-C only the larger individual azurite particles could be distinguished, whereas the finer grains were completely covered by egg yolk/rabbit glue, added either during the pigment or the paint preparation. Some large circular pockmarks could be observed on the paint surface, as relics of air bubbles.

After the UV-aging test, dosimeters with the coarser pigments (Fig. 1b, e, h) displayed a whitish glaze with a slight yellowish tint on the surface, which was more pronounced in AZ-M-C. Instead AZ-EF-C (Fig. 1k) suffered severe discoloration towards yellow, while a less significant color change took place on AZ-ST-C (Fig. 1n). Here, part of the organic binder was lost, thus a larger amount of the fine grained azurites was now discernible. Furthermore, some surface micro-pitting was observed which at first might seem surprising considering the low RH conditions (i.e., 25 ± 10% RH) during the artificial UV-aging test. However, in this RH range the amount of water absorbed by the glue changes drastically. Karpowicz [41] reported that below 30% RH, the protein molecule surface was covered only by a monomolecular layer of water. In contrast, above this RH the proteins contained more water, reaching 0.3–0.5 g of water per 1 g of protein at 30–90% RH. With this in mind, and considering that the paint dosimeters were at times exposed to RH >30%, a significant increase in moisture content of the glue binder could be expected, which facilitated dissolution processes leading to the formation of micro-pitting on the sample surface.

The two-year outdoor exposure caused binder and pigment loss in all paint dosimeters, being more significant in AZ-EF-C and AZ-ST-C (Fig. 1l). AZ-ST-C revealed a very distinct surface appearance compared with the blank dosimeter (Fig. 1o). Individual pigments were no longer covered by egg yolk/rabbit glue binders, thus morphological features of crystals were perfectly seen. The surface also suffered micro-pitting and formation of fine fissures.

3.2. Particle size analysis of powder pigments

Particles in powder pigments are hardly uniform in size. Results revealed a wider particle size range (Fig. 2, Table 3) as compared to manufacturer's data (see Table 1). However, it should be said that this technique might detect larger particle sizes, due to the aggregation of smaller particles. Indeed, note that stereomicroscope and SEM observation did not show particles >100 μm. Generally, the finer pigments (AZ-EF and AZ-ST) have wider particle size ranges than do coarser pigments (Fig. 2), especially in the case of AZ-ST which has many particles <10 μm, down to ca. 0.2 μm. Our results agree with the finding of Han et al. [27] who noticed the existence of nanometer-sized particles in diverse historical azurite pigment grades; these were more abundant and finer in size in the smaller particle-size azurites and greatly influence their luminosity.

3.3. Thermogravimetric analysis of pigments and dosimeters

Using TG analyses the egg yolk content added to the azurites during the Michel Price method, as well as the rabbit glue binder added to prepare the paint dosimeters were determined. The former was estimated taking into account the weight loss upon heating from 50 to 200 °C, considering the weight loss of pure egg yolk in the same temperature range (Table 4). Note that weight loss data <50 °C were not considered for calculating the egg yolk content because loss is mainly caused by adsorbed water. Results showed that the egg yolk content was highest in AZ-ST (10.5 wt%) compared with the other pigments (ranging from 2 to 3.5 wt%).

The rabbit glue binder content was calculated from the TG weight loss data (50–950 °C) considering the weight loss of the corresponding pigment and pure binder in the same temperature

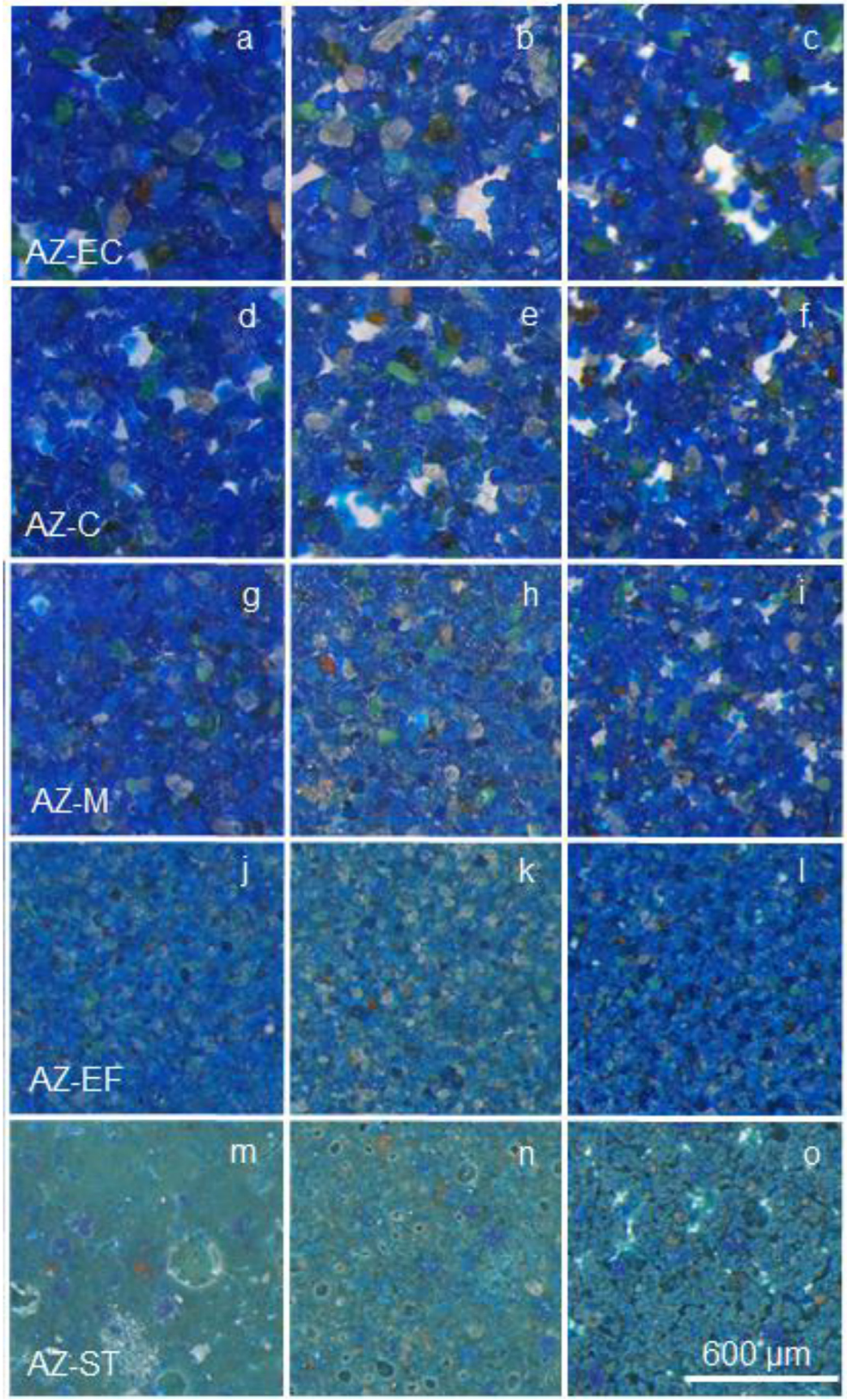

Fig. 1. Stereomicroscope photographs of azurite-proteinaceous paint dosimeters: (a, d, g, j, m) blank, (b, e, h, k, n) artificial UV-aged, (c, f, i, l, o) outdoor sunlight exposed.

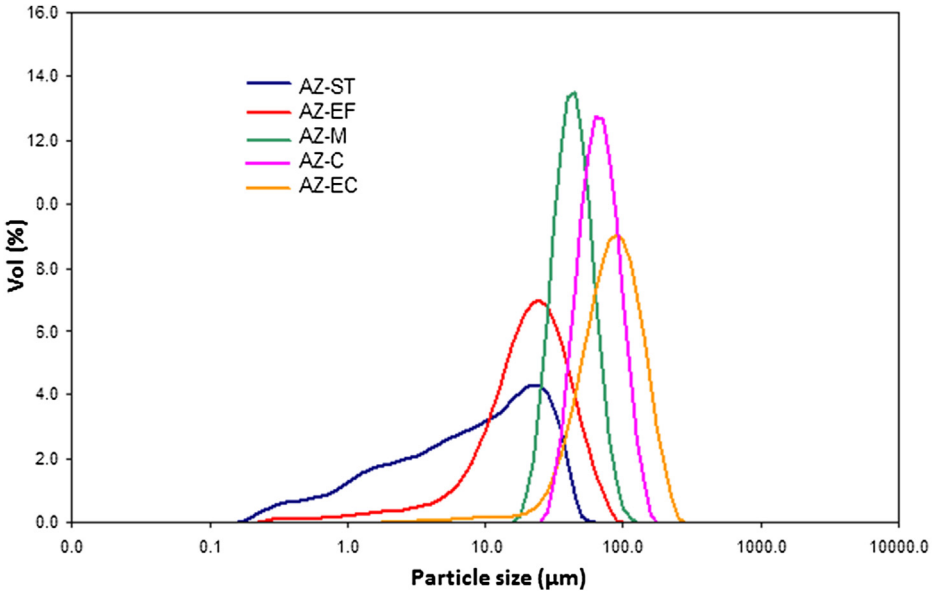

Fig. 2. Particle size distribution of azurite pigments.

Table 3
Particle size (μm) of azurite pigments studied in this work.

Pigment	Main Maximum (Authors)	Range (Authors)	Range (Kremer)
AZ-EC	90	20–280	80–100
AZ-C	70	25–180	63–80
AZ-M	45	20–110	38–63
AZ-EF	25	4–90	<38
AZ-ST	22	0.2–55	<120

range. It was found that binder content generally increased with decreasing pigment size (Table 4). However, the calculated amount of rabbit glue binder was unexpectedly low in AZ-ST-C (i.e. 8.4 wt%), considering that this dosimeter is made of the finest particles. Nevertheless, it has to be kept in mind that the AZ-ST pigment already contained a high quantity of egg yolk (10.5 wt%), added during its preparation by the manufacturer; hence the AZ-ST-C dosimeter had the highest amount of total organic media (18 wt%).

After the two-year outdoor exposure, paint dosimeters suffered a decrease in organic content of ~50–60%. Note that this technique did not allow determining whether the reduction was primarily due to egg yolk or rabbit glue loss. No relation was observed between organic content decrease and pigment size.

3.4. XRD of pigments and dosimeters

The diffraction patterns of azurite pigments revealed the presence of mineral phases matching the following Joint Committee on Powder Diffraction Standards (JCPDS): azurite (JCPDS card no 701579), malachite (JCPDS card no 760660) and quartz (JCPDS card no 331161), these last two present as impurities. Semi-quantitative (~5%) XRD analyses (Table 5) showed that the azurite content was highest in AZ-ST (90%) and lowest in AZ-EF (70%). Note that XRD analyses of two different batches of AZ-ST are shown in Table 5, displaying different mineralogical composition, which indicates that quality control for this pigment could be improved. In this work only AZ-ST-1 was used.

XRD analyses showed that no mineralogical changes took place upon UV-aging. Bragg peak positions of sunlight exposed samples did not change either; thus evidence for an azurite to malachite transformation was not detected using this technique. However, XRD patterns of the latter revealed an additional peak at ~3.03 Å indicating the presence (~10 wt%) of calcite ($CaCO_3$, JCPDS card no 050586), likely due to the deposition of particulate matter on the dosimeters' surface. Note that Ca and Mg carbonates are among the major mineral phases detected in soil dust in Granada [14,37]. Considering the low reactivity and hygroscopicity of calcite, alteration processes are not likely to be accelerated by its presence. However, it will affect the esthetic perception of the painted surface.

3.5. SEM-EDX of paint dosimeters

SEM-EDX analyses of blank azurite dosimeters revealed the presence of mainly copper (Cu) and in minor amounts silicon (Si), aluminum (Al), iron (Fe), barium (Ba), sulfur (S), calcium (Ca), potassium (K) and titanium (Ti). A general spectrum based on five EDX analyses taken from the AZ-C-C dosimeter is shown in Fig. 3a. Using false-color phase mapping (Fig. 3b) these elements were related

Table 4
Egg yolk content (wt%) of commercial pigments and rabbit glue binder content (wt%) of blank and outdoor exposed dosimeters, calculated based on TG data.

Commercial Pigments	Egg yolk content of commercial pigments	Dosimeters	Rabbit glue binder content in blank dosimeters	Total organic content in blank dosimeters	Organic content of dosimeters after 2-year outdoor exposure
AZ-EC	2.3	AZ-EC-C	7.9	10.0	6.1
AZ-C	2.9	AZ-C-C	7.7	10.4	5.4
AZ-M	3.5	AZ-M-C	8.8	12.0	6.9
AZ-EF	2.0	AZ-EF-C	9.3	11.1	5.3
AZ-ST	10.5	AZ-ST-C	8.4	18.0	10.0

Table 5
Mineralogical composition (wt%) of azurite pigments according to semi-quantitative (~5%) XRD analysis.

Pigment	Azurite (JCPDS 701579)	Malachite (JCPDS 760660)	Quartz (JCPDS 331161)
AZ-EC	80	10	10
AZ-C	85	5	10
AZ-M	85	5	10
AZ-EF	70	>5	20
AZ-ST-1	90	<5	<5
AZ-ST-2	50	10	40

Note: 1 and 2 refer to two different batches of "azurite natural standard" pigment acquired from Kremer Pigments GmbH & Co. KG.

with the following mineral phases: azurite, quartz, aluminum silicates (ascribed to clay minerals as impurities) [42], barite ($BaSO_4$), calcite ($CaCO_3$), iron-bearing oxides/hydroxides, and dolomite ($CaMg(CO_3)_2$). Mapping also provided information on binder distribution.

SEM images of blank dosimeters revealed that the coarser pigments were covered with a thin rabbit glue binder layer which conferred a smooth, rounded aspect to the originally sharp edges of azurite particles (Fig. 4a, d, g). The relatively large pores between individual azurite particles were filled with binder. In the case of dosimeters prepared with finer pigments (AZ-EF-C and AZ-ST-C), discrete pigment particles could rarely be distinguished, thus the paint appeared as a homogeneous mixture of pigments and binder (Fig. 4j, m). Additionally some drying cracks were observed in AZ-EF-C (Fig. 4).

The artificial UV-aging test caused severe first- and second-order polygonal cracking in the glue binder present in dosimeters prepared with the coarser pigments (Fig. 4b, e, h). In contrast, crack formation was very limited in dosimeters containing the finest pigments (Fig. 4k, n). Cracks were quantified using image analysis (Table 6). Calculated data showed that the linear crack density decreased with decreasing particle size. Quantification could not be done in AZ-ST-C since this paint suffered significant superficial binder loss. AZ-EF-C also suffered some binder loss during UV-irradiation. Consequently in both dosimeters discrete azurite particles were distinguished. Moreover, in AZ-ST-C some micro-pitting was observed which has also been detected in stereomicroscopic images (Fig. 1n).

Crack formation can be attributed to RH fluctuations during the UV-aging test. It can, to a large degree, be correlated with the binder distribution in paint dosimeters. The accumulation of larger amounts of glue in pores of dosimeters prepared with coarse pigments resulted in severe cracking upon UV-aging. Finer pigment particles ($\phi < 25$ μm, present in e.g. AZ-ST-C), in contrast, facilitated a more homogeneous pigment and binder distribution, thus reducing crack development caused by volume changes of the binder. Cracking, causing an increase in the paint's surface area, further facilitates accelerated chemical and physical attack. Moreover, organic and inorganic particle matter can accumulate in these cracks, enhancing or catalyzing degradation.

After two-year outdoor exposure all paint dosimeters (except AZ-ST-C) suffered severe binder loss. Hence pigments appeared completely uncovered by glue, and thus sharp particle edges, as well as empty pores, could now be observed (Fig. 4l). AZ-ST-C also experienced some superficial binder loss, and likewise, larger azurite particles (~10 μm) are now discernible. However, due to the high organic content of this paint, some egg yolk/rabbit glue were still retained and cemented small azurite particles (i.e., <1 μm), which formed compact aggregates (Fig. 4o). Overall, SEM did not reveal any alteration of azurite pigments; only the organic binder (egg yolk or rabbit glue) seemed to have been affected by the artificial UV-aging or the long-term outdoor exposure.

3.6. Chromatic features of paint dosimeters

Spectrophotometry results revealed that L* and C* of blank dosimeters generally increased with decreasing particle size of azurite pigments (Table 7). The exception was AZ-ST-C which showed the lowest values (L* = 37.12 and C* = 15.82), in spite of its particle size. This behavior was attributed to its high organic content (both egg yolk and rabbit glue). Diminishing crystal size also induced dosimeters to turn more greenish, since a* values vary from 2.59 (AZ-EC-C) to −10.13 (AZ-ST-C). Data also showed that AZ-M-C was the bluest sample (b* = −32.45) while AZ-ST-C was the greenest (a* = −10.13). The particularly high a* value of AZ-ST-C is also attributed to the high organic content, particularly due to the egg yolk amount added during its preparation by the manufacturer. Thus AZ-ST-C is very dissimilar in color parameters to the other dosimeters (see Fig. 1).

Color changes were more severe in dosimeters exposed to

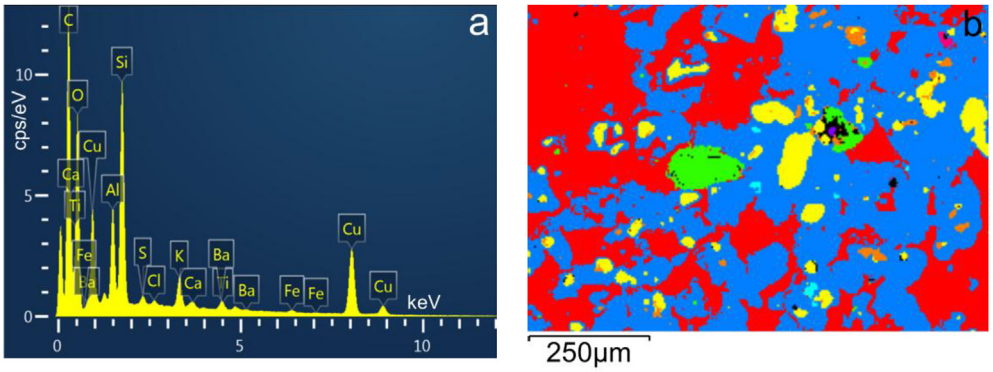

Fig. 3. AZ-C-C dosimeter: a) general EDX spectrum, b) SEM-EDX false-color mineral map. Blue = azurite, red = glue, yellow = quartz, orange = aluminum silicates, green = barite, violet = dolomite, pink = iron-bearing oxides/hydroxides, and light blue = KCl phase. (For interpretation of the references to color in this figure legend, the reader is referred to the web version of this article.)

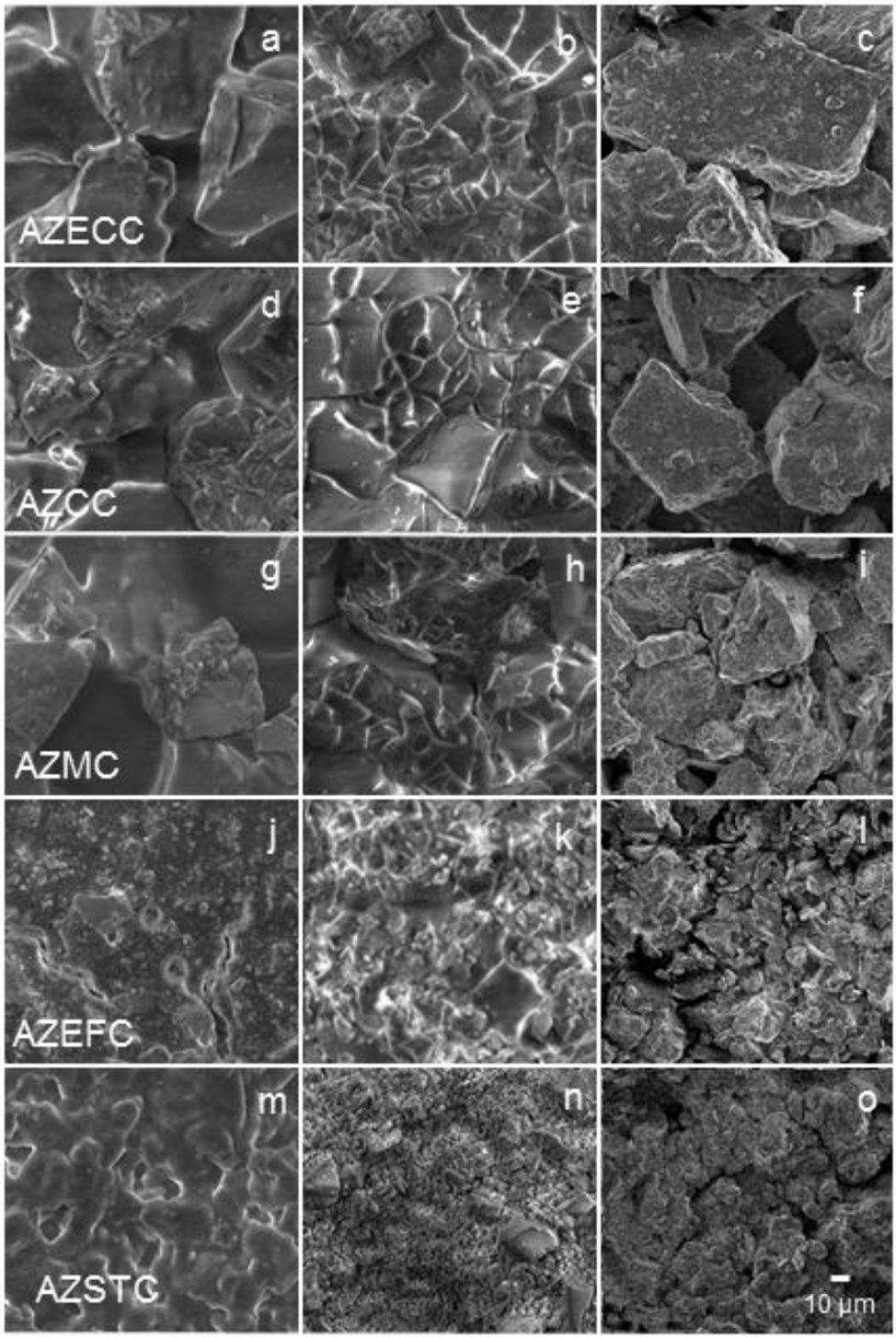

Fig. 4. SEM photographs of blank (a, d, g, j, m), UV-aged (b, e, h, k, n) and 2-year outdoor exposed (c, f, I, l, o) azurite-proteinaceous dosimeters.

Table 6
Crack formation (linear crack density, mm^{-1}) in paint dosimeters upon UV aging.

Paint dosimeter	Linear crack density
AZ-EC-C-UV	88
AZ-C-C-UV	68
AZ-M-C-UV	51
AZ-EF-C-UV	34
AZ-ST-C-UV	Not available

1000 h of artificial UV radiation as compared to samples after two-year outdoor exposure (Fig. 1). The former samples experienced $\Delta E = \sim 10–17$ units, which increased with decreasing pigment particle size. This color change was attributed to deterioration of the organic binders added to the azurites, which caused a substantial decrease in a^* and an increase in b^* (i.e., a shift towards green/yellow). However, AZ-ST-C behaved differently and only suffered $\Delta E = 6$ units. In this paint the yellowish color of the original pigment containing ~10% egg yolk, may have partially

Table 7
Chromatic parameters: luminosity (L*), a* and b* (chromatic coordinates), chroma (C*), h* (hue), and their corresponding shift, i.e. ΔL* (lightness/darkness), Δa* (redness/greenness), Δb* (yellowness/blueness), ΔC* (saturation), and total color variation (ΔE) for blank and aged dosimeters exposed to artificial UV irradiation and outdoor sunlight. Standard deviations are included.

Dosimeters	L*	a*	b*	C*	h*	ΔL*	Δa*	Δb*	ΔC*	ΔE
AZ-EC-C	33.11 ± 0.22	2.59 ± 0.21	−28.26 ± 0.28	28.38 ± 0.30	275.23 ± 0.38					
AZ-C-C	34.70 ± 0.26	3.24 ± 0.16	−29.54 ± 0.38	29.72 ± 0.23	276.25 ± 0.23					
AZ-M-C	37.28 ± 0.20	2.33 ± 0.05	−32.45 ± 0.22	32.54 ± 0.07	274.10 ± 0.07					
AZ-EF-C	42.37 ± 0.19	−5.82 ± 0.05	−29.60 ± 0.12	30.17 ± 0.13	258.89 ± 0.13					
AZ-ST-C	37.12 ± 0.03	−10.13 ± 0.01	−12.16 ± 0.09	15.82 ± 0.22	230.20 ± 0.22					
AZ-EC-C-UV	33.19 ± 0.48	−2.01 ± 0.37	−19.41 ± 0.72	19.51 ± 0.70	264.06 ± 1.19	0.17 ± 0.51	−4.60 ± 0.36	8.88 ± 0.71	−8.89 ± 0.69	10.02 ± 0.73
AZ-C-C-UV	35.55 ± 0.43	−2.88 ± 0.13	−18.52 ± 0.30	18.75 ± 0.31	261.17 ± 0.37	0.93 ± 0.43	−6.10 ± 0.13	11.03 ± 0.29	−10.99 ± 0.29	12.65 ± 0.25
AZ-M-C-UV	38.38 ± 0.86	−5.04 ± 0.12	−17.91 ± 0.33	18.61 ± 0.29	254.29 ± 0.60	1.09 ± 0.86	−7.36 ± 0.12	14.54 ± 0.33	−13.93 ± 0.29	16.36 ± 0.38
AZ-EF-C-UV	45.04 ± 0.25	−11.77 ± 0.23	−13.67 ± 0.26	18.04 ± 0.17	229.26 ± 0.92	2.67 ± 0.25	−5.96 ± 0.23	15.93 ± 0.26	−12.12 ± 0.17	17.22 ± 0.30
AZ-ST-C-UV	37.99 ± 0.49	−11.23 ± 0.31	−6.19 ± 0.48	12.83 ± 0.43	208.85 ± 1.66	0.87 ± 0.49	−1.10 ± 0.31	5.97 ± 0.48	−3.00 ± 0.43	6.15 ± 0.47
AZ-EC-C-2Y	35.70 ± 0.25	0.88 ± 0.07	−25.72 ± 0.29	25.74 ± 0.29	271.96 ± 0.17	2.59 ± 0.25	−1.71 ± 0.07	2.54 ± 0.29	−2.64 ± 0.29	4.03 ± 0.14
AZ-C-C-2Y	36.69 ± 0.20	0.60 ± 0.04	−24.55 ± 0.27	24.56 ± 0.27	271.39 ± 0.09	1.99 ± 0.20	−2.64 ± 0.04	4.99 ± 0.27	−5.16 ± 0.27	5.99 ± 0.18
AZ-M-C-2Y	36.56 ± 0.34	0.15 ± 0.13	−27.33 ± 0.55	27.33 ± 0.55	270.31 ± 0.27	−0.72 ± 0.34	−2.18 ± 0.13	5.12 ± 0.55	−5.21 ± 0.55	5.62 ± 0.59
AZ-EF-C-2Y	47.70 ± 0.43	−6.22 ± 0.14	−29.12 ± 0.66	29.78 ± 0.62	257.94 ± 0.53	5.33 ± 0.43	−0.40 ± 0.14	0.48 ± 0.66	−0.39 ± 0.62	5.40 ± 0.53
AZ-ST-C-2Y	47.01 ± 0.40	−10.99 ± 0.32	−11.14 ± 0.51	15,65 ± 0,58	225.39 ± 0.53	9.89 ± 0.40	−0.86 ± 0.32	1.02 ± 0.51	−0.17 ± 0.58	10.00 ± 0.39

masked the green/yellow color change induced by rabbit glue aging.

The two-year outdoor exposure of dosimeters resulted in ΔE = 4–6 units which could not be correlated with the pigment particle size, and was induced by a decrease in a* (towards green) and a minor increase in b* (towards yellow). Moreover L* increased with decreasing particle size, mostly in AZ-EF-C and AZ-ST-C (values ~47); also L* was in most cases slightly higher than that attained in the UV-aged dosimeters. Again, AZ-ST-C behaved differently, experiencing a ΔE = 10 units caused by a significant increase in L* which was attributed to the binder/egg yolk loss in the dosimeter's surface, leaving pigments uncovered. Assuming that color change is mainly caused by binder degradation, the superficial binder loss explains the smaller color change experienced by dosimeters after two-year outdoor exposure, as compared to samples exposed to artificial UV aging where, in general, no important binder loss has been detected.

3.7. Raman analysis

Raman analysis was performed on pigments, binder and dosimeters. Low quality spectra were acquired from pure organic rabbit glue binder with the two laser excitations. Results from azurite-glue dosimeters showed that bands corresponding to this binder – appearing in the region between 2800 and 3000 cm^{-1} – were only visible in blank dosimeters when spectra were acquired with the green laser (Fig. 5). These bands, which can be related to the ν(CH) stretching mode of proteins from the proteinaceous glue, did not appear in any of the aged dosimeters, irrespective of the laser excitation used. Hence ATR-FTIR was used to study in-depth changes taking place within the organic binder (see Section 3.8).

Raman spectra of powder pigments where similar in all azurite grades. Moreover, we could not relate the line-width of the Raman band at ~400 cm^{-1} with particle size as proposed elsewhere [27]. The azurite Raman bands could be detected in blank and aged dosimeters using both lasers. However, bands were better seen with the green laser, despite the high fluorescence compared with that observed in spectra acquired with the red laser. Here we show the Raman spectra of the blank and aged AZ-C-C dosimeters (representative of all samples) acquired with the green laser.

Azurite Raman bands (Fig. 5a) were assigned according to published data [27,43,44]. Fig. 5b displays the Raman spectrum of the UV-aged AZ-C-C dosimeter, and shows clearly that fluorescence masks the azurite Raman bands, displaying lower intensity. Also, a shift towards higher wavenumbers is observed in certain azurite bands (i.e. 248, 285, 761, 829, 933 cm^{-1}) up to 1096 cm^{-1}. Above this wavenumber the azurite bands are missing, as are those credited to the organic binder. The patent shift of these bands could be due to a variation in the chemical bond length of certain bonds in the azurite molecule (causing a structural change) triggered by the UV irradiation.

Fig. 5c shows the Raman spectrum of the outdoor exposed AZ-C-C dosimeter. Here the fluorescence is lower than that found in both the blank and the UV- aged dosimeters. This striking result can easily be explained when observing the SEM images of the corresponding dosimeters (Fig. 4). In all blank and UV-aged dosimeters, the azurite pigments are surrounded by the binder (different extension according to azurite grade), which contributes to Raman fluorescence. In addition, in the UV-aged dosimeters cracks formed (to different degrees, according to crystal size) in the binder. UV-induced protein fragmentation causes an increased amount of short chains which should have contributed to the increase in fluorescence. By contrast, in outdoor aged dosimeters severe binder loss is observed in SEM images, such that uncovered azurite crystals are clearly seen. Thus, the spectra of these dosimeters show the lowest fluorescence and the most intense azurite bands of all dosimeters.

Fig. 5c also reveals that some blue crystals gave spectra where two extra Raman signals appeared at 466 and 1049 cm^{-1}, which correspond to malachite. The Raman spectra of malachite and azurite are very similar. According to literature, the three typical bands of malachite are identified at 435 cm^{-1} corresponding to the lattice modes T (Cu,CO_3; not seen here), and at 1049 and 1097 cm^{-1} related to the ν_1 symmetric stretching modes (of two different CO_3 groups - doubly degenerate mode) [45].

Malachite is a natural impurity present in azurite mineral. Indeed, in this work malachite has been identified with XRD in all pigments (Table 5). Malachite can also be a weathering product of azurite since it is more stable than azurite under atmospheric conditions [46]. That is, azurite is more prone to oxidation processes, and, in the presence of water slowly transforms into malachite. Malachite is a pseudomorph of azurite that holds the same external form as the original azurite crystal, but the unit cells of azurite are gradually replaced by those of malachite. Thus, during this process crystals with intermediate chemical compositions between azurite and malachite can be found, as recognized here.

The Raman spectra acquired from paint dosimeters exposed during two-year to the urban atmosphere of Granada, show a mineral phase intermediate in composition between that of azurite and malachite (Fig. 5c), as also found by Salvadó et al. [47]. We

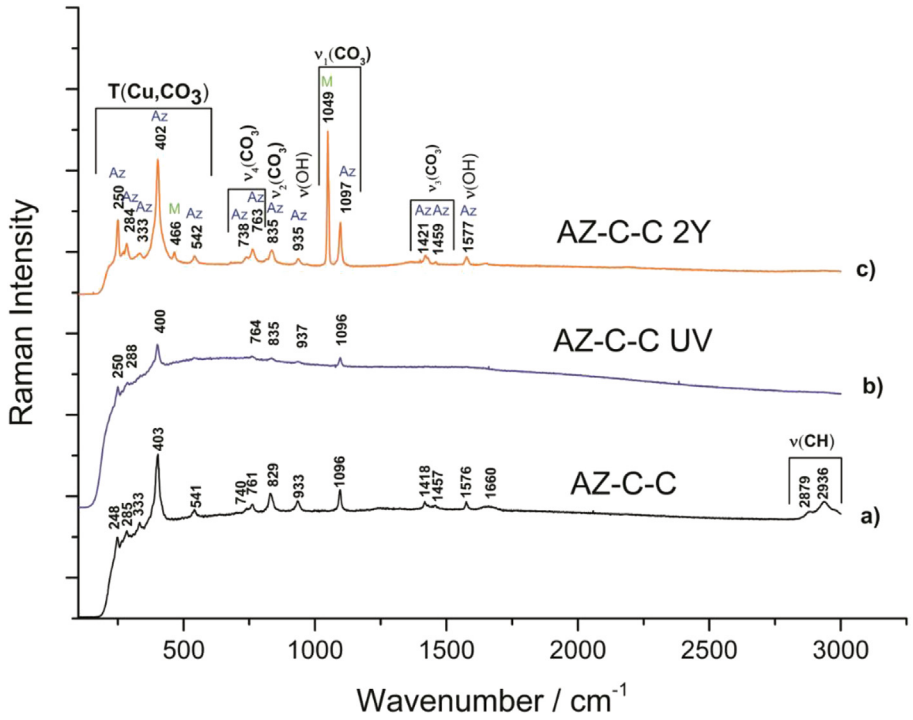

Fig. 5. Raman spectra (green laser) of blank, UV-aged and sunlight-aged AZ-C-C dosimeters. T = torsion, M = malachite, Az = azurite. (For interpretation of the references to color in this figure legend, the reader is referred to the web version of this article.)

discount the hypothesis that this intermediate phase was part of the original pigment since it was not found in the blank dosimeters or in the UV-aged ones (Fig. 5). Malachite formation should have been minimal since semi-quantitative XRD analysis (~5%) on two-year aged paints detected no changes compared to the blank dosimeters.

3.8. ATR-FTIR analysis

ATR-FTIR results revealed that the amide I band (carbonyl stretching) and amide II band (N—H bending) of the proteinaceous binder were modified in blank dosimeters. The amide I band at 1627 cm^{-1} shifted to 1640-1645 cm^{-1} when blended with the different azurite grades (Table 8). This band is caused mainly (~80%) by C═O stretching vibrations of the peptide linkages of amino acids [48], and is absent in pure azurite pigments (see AZ-C in Fig. 6). The shift corresponds to a blue shift associated with a frequency increase ($\Delta\sigma = 20$ cm^{-1}) which indicates increased bond strength of C═O groups (i.e., the bond dissociation strength increases) [49].

The frequency of the amide I band, and thus, the bond strength of C═O groups, is influenced by intra- and intermolecular hydrogen bonding of peptides [50]. When a reduction in hydrogen bonds between N—H and C═O groups of protein chains takes place, the frequency increases subsequently. According to Kong and Yu [48] this shift indicates changes in the secondary structure from β-sheets to random coils. Hence, the decrease in hydrogen bonds in the azurite-glue paints, as compared to pure glue, can be explained by the formation of protein-Cu^{2+} complexes occupying N—H groups of the protein chains, thus reducing sites for hydrogen bonding [19]. Our results agree with the findings of Odlyha et al. [18], who stated that copper catalyzed the oxidation of the egg yolk binder prior to light aging of azurite tempera dosimeters.

FTIR data showed that the amide I band shift was slightly larger in paints prepared with fine grained pigments than with coarser pigments. Although observed differences are small, all pigments followed the same tendency; thus, results suggest that the binder-pigment interaction might have been stronger in the case of fine grained pigments. This seems reasonable considering that smaller pigment particles offer a larger surface area for reaction with amino acids in the glue binder as compared with coarser pigments. On the other hand, the amide II band at 1529 cm^{-1} shifted to 1492-1502 cm^{-1} when blending the binder with the different azurites (Table 8). The observed significant red shift is considered to be a clear indication of the complexation of Cu^{2+} ions with the amide group, a process that reduces the frequency of the bending vibrations of these C—N bonds through the attachment of heavier atoms [51,52].

Upon UV-exposure for 1000 h, the amide I and amide II bands of

Table 8
ATR-FTIR wavenumbers of amide I and amide II bands (cm^{-1}) identified on blank, UV-aged, and outdoor-aged glue and paint dosimeters.

Dosimeter	Amide I	Amide II
Rabbit Glue	1627	1529
Rabbit Glue-UV	1628	1531
Rabbit Glue 2Y	1628	1528
AZ-EC-C	1640	1498
AZ-EC-C-UV	1651	1497
AZ-EC-C-2Y	1653 (vw)	1488
AZ-C-C	1642	1494
AZ-C-C-UV	1651	1506
AZ-C-C-2Y	1653 (vw)	1488
AZ-M-C	1642	1502
AZ-M-C-UV	1647	1502
AZ-M-C-2Y	1656 (vw)	1488
AZ-EF-C	1645	1492
AZ-EF-C-UV	1649	1497
AZ-EF-C-2Y	1651	1488
AZ-ST-C	1645	1492
AZ-ST-C-UV	1651	1488
AZ-ST-C-2Y	1653 (vw)	1490

vw = very weak.

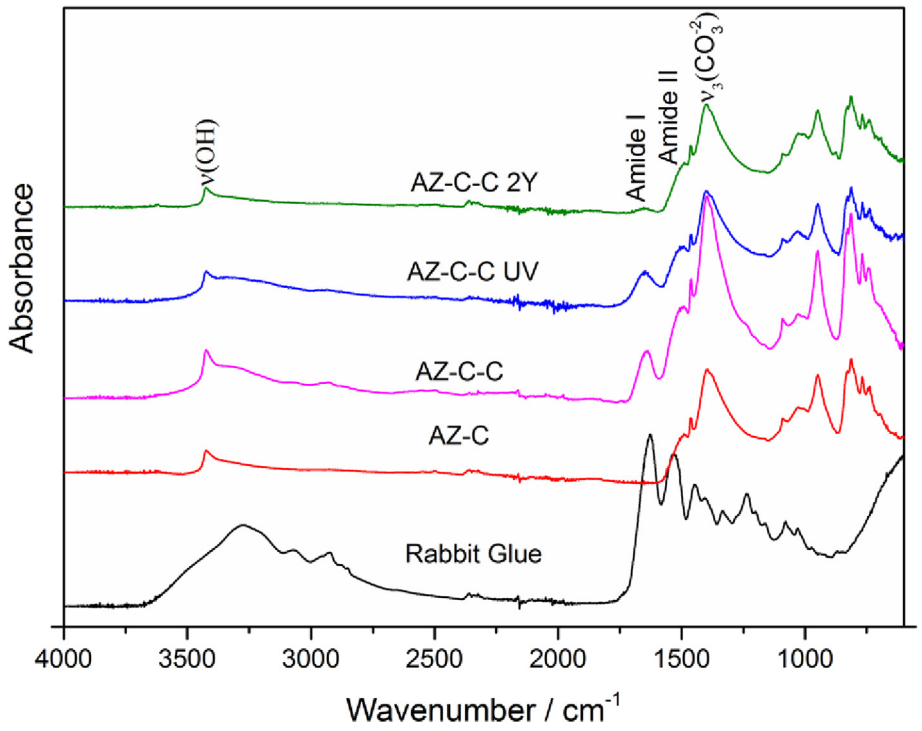

Fig. 6. ATR-FTIR spectra of blank rabbit glue, azurite coarse pigment, and blank, UV-aged and two year sunlight-aged AZ-C-C dosimeters.

the pure rabbit glue dosimeters did not suffer any important shift (Table 8). Thus, the spectra of the blank and UV-aged glue samples are quite similar (Fig. 7). However, changes in the intensity ratio of bands at ~1028 and ~1076 cm^{-1}, associated with C—O bonds occurred, indicating a modification of the conformational structure of the rabbit glue binder.

The amide I band appearing in the paint dosimeters suffered a shift to higher frequencies (Table 8, Fig. 6), which indicates a decrease in hydrogen bonding due to the UV irradiation. This suggests that the presence of azurite induced the breaking of hydrogen bonds since the position of the amide I band in pure glue did not change. The shift was more noticeable in paint dosimeters made of larger particle size. Note that the breaking of hydrogen bonds will influence the glue's adhesive power and elasticity negatively [53]. These results are in agreement with findings by Ghezzi et al. [54], who also detected changes in the glue's behavior

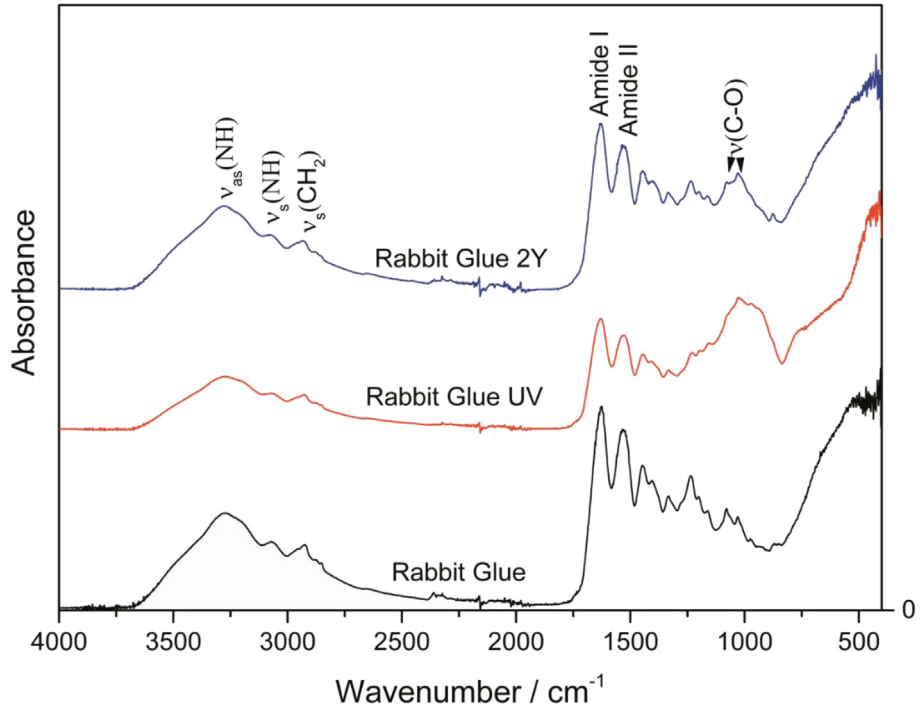

Fig. 7. ATR-FTIR spectra of blank, UV-aged and two year sunlight-aged rabbit glue dosimeters.

upon mixing with azurite pigment. According to these authors, the glue-azurite mixture showed less thermal stability than pure glue, which they attributed to conformational changes. In azurite paint dosimeters the amide I band and the band at ~3300 cm^{-1} corresponding to N–H stretching did not change significantly as compared with the blank paint dosimeters (Fig. 6). This suggests that binder loss was limited in paint dosimeters exposed to 1000 h UV radiation, as observed in SEM images.

The two-year outdoor test caused a significant alteration of the rabbit glue binder in the paint dosimeters, as shown by a drastic decrease or even absence of several bands related to peptide linkage (the amide I band and the band at ~3300 cm^{-1}) (Fig. 6). These results agree with the stereomicroscopic and SEM observations (Fig. 4c, f, i, l, o) and TG results, revealing a severe binder loss in outdoor-exposed dosimeters, which could be attributed to dissolution caused by condensation. Nonetheless, the shifts detected in the very low intensity amide I bands in outdoor-aged dosimeters were in most cases similar to those detected in the UV-aged dosimeters (Table 8), even though the light exposure duration and irradiance level were significantly higher during the two-year outdoor exposure.

4. Conclusions

Particle size influenced the binder distribution in azurite tempera dosimeters, which controlled crack formation in paints during accelerated UV-aging. Paints made of coarse pigments were especially prone to crack formation. Thus we conclude that mixing these pigments with a small quantity of fine-grained azurites (i.e., AZ-EF) would be beneficial to avoid crack formation. Finer grains can fill pore spaces between coarse pigments, preventing large accumulations of rabbit glue, and thus reducing binder volume changes caused by RH and/or T variations. However, the amount added must be kept to a minimum in order to preserve the color properties and limit binder-pigment interactions since, as revealed by FTIR data, interactions were stronger in fine-grained azurite paints leading to conformational structural changes of the binder. Changes in the binder structure are most likely responsible for the color variation towards yellow/green of the UV-aged paints, which was more severe as the pigment particle size decreased, since the binder demand increased.

Overall, color changes of paint dosimeters were related to binder degradation. Although color variations perceptible to human eye were found in all light-aged paints, they were lower in outdoor exposed dosimeters due to binder loss exposing unaltered azurite crystals. However, the identified transformation of azurite into malachite in paints exposed outdoors might add to the color change upon long-term exposure, as well as deposition of calcite particles from soil dust.

Experimental results also show the importance of a detailed characterization of painting materials prior to scientific investigations or applications in conservation treatments. Until now little has been published in this respect, although optical, chemical and physical properties might vary significantly with impurities or quality variations among different batches of pigments or binders, which will influence pigment-binder interactions, and thus, the paint aging behavior. These aspects deserve special consideration since they will have important implications in the outcome of aging studies and also affect the durability of conservation treatments of (wall)paintings.

Acknowledgements

Financial support was provided by Spanish Research Projects AERIMPACT (CGL2012-30729) and EXPOAIR (P12-FQM-1889), the European Regional Development Fund (ERDF), and the Andalusian Research Group RNM-179. Analyses were performed in the Scientific Instrumentation Centre (CIC) of the University of Granada. J.A. Herrera is funded by a Spanish grant from the AERIMPACT Project (ref.BES-2013- 065507), and K. Elert is a post-doctoral researcher in the EXPOAIR Project. The authors thank R. Gutiérrez for helping with the UV-aging test, and A. Kowalski for English revision.

References

[1] Cardell C, Rodríguez-Simón L, Guerra I, Sánchez-Navas A. Analysis of Nasrid polychrome carpentry at the Hall of the Mexuar palace, Alhambra complex (Granada, Spain) combining microscopic, chromatographic and spectroscopic methods. Archaeometry 2009;51:637–57.
[2] Comelli D, Nevin A, Valentini G, Osticioli I, Mario Castellucci E, Toniolo L, et al. Insights into Masolino's wall paintings in Castiglione Olona: advanced reflectance and fluorescence imaging analysis. J Cult Herit 2011;12:11–8.
[3] Romero-Pastor J, Durán A, Rodríguez-Navarro AB, Van Grieken R, Cardell C. Compositional and quantitative microtextural characterization of historic paintings by means of micro-X-ray diffraction and Raman microscopy. Anal Chem 2011;83:8420–8.
[4] Gómez-Morón MA, Ortiz P, Martín-Ramírez JM, Ortiz R, Castaing J. A new insight into the vaults of the kings in the Alhambra (Granada, Spain) by combination of portable XRD and XRF. Microchem J 2016;125:260–5.
[5] Durán A, Franquelo ML, Centeno MA, Espejo T, Pérez-Rodríguez JL. Forgery detection on an Arabic illuminated manuscript by micro-Raman and X-ray fluorescence spectroscopy. J Raman Spectrosc 2011;42:48–55.
[6] Hradil D, Píšková A, Hradilová J, Bezdicka P, Lehrberger G, Gerzer S. Mineralogy of bohemian green earth pigment and its microanalytical evidence in historical paintings. Archaeometry 2011;53:563–86.
[7] Cardell C. Painting materials and technical evolution of Islamic polychrome art of the Nasrid Dynisty in Granada, Spain. In: Hradil D, Hradilová J, editors. Acta artis academica: knowledge and experience in the fine art. Prague: Academy of Fine Arts; 2012. p. 9–24.
[8] Wang N, He L, Egel E, Simon S, Rong B. Complementary analytical methods in identifying gilding and painting techniques of ancient clay-based polychromic sculptures. Microchem J 2014;114:125–40.
[9] Dei L, Ahle A, Baglioni P, Dini D, Ferroni E. Green degradation products of Azurite in wall paintings: identification and conservation treatment. Stud Conserv 1998;43:80–8.
[10] Manzano E, Romero-Pastor J, Navas N, Cardell C. A study of the interaction between rabbit glue binder and blue copper pigment under UV radiation: a spectroscopic and PCA approach. Vibrat Spectrosc 2010;53:260–8.
[11] Anaf W, Trashin S, Schalm O, van Dorp D, Janssens K, De Wael K. Electrochemical photodegradation study of semiconductor pigments: influence of environmental parameters. Anal Chem 2014;86:9742–8.
[12] Giacopetti L, Satta A. Degradation of Cd-yellow paints: ab initio study of native defects in {10.0} surface CdS. Microchem J 2016;126:214–9.
[13] Herrera Rubia A, Navas N, Cardell C. An evaluation of the impact of urban air pollution on paint dosimeters by tracking changes in the lipid MALDI-TOF mass spectra profile. Talanta 2016;155:53–61.
[14] Horemans B, Cardell C, Bencs L, Kontozova-Deutsch V, DeWael K, Van Grieken R. Evaluation of airborne particles at the Alhambra monument in Granada. Spain Microchem J 2011;99:429–38.
[15] Douglas-Jones R, Hughes JJ, Jones S, Yarrow T. Science, value and material decay in the conservation of historic environments. J Cult Herit 2016;21:823–33.
[16] Mohanu I, Mohanu D, Gomoiu I, Barbu O-H, Fechet R-M, Vlad N, et al. Study of the frescoes in Ioneştii Govorii wooden church (Romania) using multitechnique investigations. Microchem J 2016;126:332–40.
[17] Bacci M, Picollo M, Porcinai S, Radicati B. Evaluation of the museum environmental risk by means of tempera-painted dosimeters. Thermochim Acta 2000;365:25–34.
[18] Odlyha M, Cohen NS, Foster GM, West RH. Dosimetry of paintings: determination of the degree of chemical change in museum exposed test paintings (azurite tempera) by thermal analysis and spectroscopic. Thermochim Acta 2000;365:53–63.
[19] Romero-Pastor J, Navas N, Kuckova S, Rodríguez-Navarro AB, Cardell C. Collagen-based proteinaceous binder-pigment interaction study under UV aging conditions by MALDI-TOF-MS and principal component analysis. J Mass Spectrom 2012;47:322–30.
[20] Villafana TE, Delaney JK, Warren WS, Fischer MC. High-resolution, three-dimensional imaging of pigments and supporting paper and textiles. J Cult Herit 2016;20:583–8.
[21] Ballirano P, Maras A. In-situ X-ray transmission powder diffraction study of the kinetics of the light induced alteration of realgar (α-As_4S_4). Eur J Min 2006;18:589–99.
[22] Aze S, Vallet JM, Pomey M, Baronnet A, Grauby O. Red lead darkening in wall paintings: natural aging of experimental wall paintings versus artificial aging tests. Eur J Min 2007;19:883–90.
[23] Mazzeo R, Prati S, Quaranta M, Joseph E, Kendix E, Galeotti M. Attenuated total reflection micro FTIR characterisation of pigment–binder interaction in

reconstructed paint films. Anal Bioanal Chem 2008;392:65–76.
[24] Saunders D, Chahine H, Cupitt J. Long-term colour change measurement: some results after twenty years. Natl Gallery Technol Bull 1996;17:81–90.
[25] Ghelardi E, Degano I, Colombini MP, Mazurek J, Schilling M, Khanjian H, et al. A multi-analytical study on the photochemical degradation of synthetic organic pigments. Dyes Pigments 2015;123:396–403.
[26] Mattei E, Vivo G, Santis A, Gaetani C, Pelosi C, Santamaria U. Raman spectroscopic analysis of azurite blackening. J Raman Spectrosc 2008;39:302–6.
[27] Han K, Nam JY, Ji JE, Kang D, Lee H, Baek N, et al. Existence of nanoparticles in azurite and malachite pigments by Raman spectroscopy and X-ray diffraction studies. Dyes Pigments 2016;133:232–7.
[28] Price MA. Renaissance of color: particle separation and preparation of azurite for use in oil painting. Leonardo 2000;33:281–8.
[29] Gueli AM, Bonfiglio G, Pasquale S, Troja Sebastiano O. Effect of particle size on pigments colour. Color Res Appl 2016. http://dx.doi.org/10.1002/col.22062.
[30] Manzano E, Bueno AG, González-Casado A, Del Olmo M. Mortars, pigments and binding media of wall paintings in the 'Carrera del Darro' in Granada. Spain J Cult Herit 2000;1:19–28.
[31] Eastaugh N, Walsh V, Chaplin T, Siddall R. Pigment compendium: A Dictionary and optical microscopy of historic pigments. Oxford: Elsevier Butterworth-Heinemann; 2004.
[32] Kühn H. Erhaltung und Pflege von Kunstwerken und Antiquitäten 1. München: Keysersche Verlagsbuchhandlung; 1981.
[33] Merrifield M. Original treatises on the arts of paintingvol. I. New York: Dover Publications Inc.; 1967.
[34] Cennini C. The Craftsman's handbook "Il Libro dell'Arte". New York: Dover Publications Inc.; 1968.
[35] Pacheco F. Arte de la pintura. Madrid: Cátedra; 1990.
[36] Atlas weathering testing guidebook. Illinois, USA: Atlas Material Testing Technology; 2001.
[37] Urosevic M, Yebra-Rodríguez A, Sabastián-Pardo E, Cardell C. Black soiling of an architectural limestone during two-year term exposure to urban air in the city of Granada (S Spain). Sci Total Env 2012;414:564–75.
[38] Martín-Ramos JD. Using XPowder: a software package for powder X-ray diffraction analysis. 2004. GR 1001/04. ISBN 84-609-1497-6.
[39] AATCC Test Method 173-1989. CMC: calculation of small colour differences for acceptability. In: AATCC technical manual. North Carolina: american association of textile chemists and colorists; 1989.
[40] Mokrzycki WS, Tatol M. Colour change ΔE – a survey. Mach Graph Vis 2011;20:383–411.
[41] Karpowicz A. Aging and deterioration of proteinaceous media. Stud Conserv 1981;26:153–60.
[42] Aru M, Burgio L, Rumseu MS. Mineral impurities in azurite pigments: artistic or natural selection. J Raman Spectrosc 2014;45:1013–8.
[43] Frost RL, Martens WN, Rintoul L, Mahmutagic E, Kloprogge JT. Raman spectroscopic study of azurite and malachite at 298 and 77 K. J Raman Spectrosc 2002;33:252–9.
[44] Nakamoto K. Infrared and Raman spectra of inorganic and coordination compounds. Part A: theory and applications in inorganic chemistry. New York: John Wiley and Sons; 1997.
[45] Buzgar N, Apopei AI. The Raman study on certain carbonates. Analele Stiintifice ale Universitatii "Al. I. Cuza" - Iasi, vol. 55; 2009. p. 97–112.
[46] Vink BW. Stability relations of malachite and azurite. Mineral Mag 1986;50:41–7.
[47] Salvadó N, Butí S, Aranda MAG, Pradell T. New insights on blue pigments used in 15th century paintings by synchrotron radiation-based micro-FTIR and XRD. Anal Methods 2014;6:3610–21.
[48] Kong J, Yu S. Fourier Transform infrared spectroscopic analysis of protein secondary structures. Acta Biochim Biophys Sin 2007;39:549–59.
[49] Kirillov SA. Novel approaches in spectroscopy of interparticle inter-actions. Vibrational line profiles and anomalous non-coincidence effects. In: Samios J, Durov VA, editors. Novel approaches to the structure and dynamics of liquids: experiments, theories and simulations. NATO science series. The Netherlands: Springer; 2004. p. 193–227.
[50] Zhao J, Shi J, Wang J. Amide-I characteristics of helical β-peptides by linear infrared measurement and computations. J Phys Chem B 2014;118:94–106.
[51] SIAS. Infrared spectroscopy (IR). Royal Society of Chemistry; 2009.
[52] Jhaumeer-Laulloo S, Bhowon MG, Reddi K. Synthesis and characterization of benzamide metal complexes. Asian J Chem 2000;12:1296–300.
[53] Von Endt DW, Baker MT. The chemistry of filled animal glue systems. In: Bigelow D, editor. Guilded wood: conservation and historyvol. 199. Madison, Conn: Sound View Press; 1991. p. 155–62.
[54] Ghezzi L, Duce C, Bernazzani L, Bramanti E, Perla Colombini M, Tiné MR, et al. Interaction between inorganic pigments and rabbit skin glue in reference paint reconstructions. J Therm Calor 2015;122:315–22.